MINERALOGICAL MAGAZINE

VOLUME 61 NUMBER 409 DECEMBER 1997

The Minastira peraluminous granite, Puno, southeastern Peru: a quenched, hypabyssal intrusion recording magma commingling and mixing

DANIEL J. KONTAK[1] AND ALAN H. CLARK

Department of Geological Sciences, Queen's University, Kingston, Ontario, Canada K7L 3N6

Abstract

The Minastira granite, a *c.* 25 Ma subvolcanic plug of fine-grained granitic rock in the Cordillera Oriental of SE Peru, has preserved textures indicative of a history involving mixing of at least two magmas, a volumetrically dominant felsic component and a less voluminous mafic one. The felsic component is represented by variably fractured, altered and embayed crystals of quartz, feldspar, biotite with minor coarse-grained melt- and fluid-inclusion rich apatite, and possible cordierite (now a pseudomorphous Fe–Mg phase), whereas the mafic component is represented by calcic plagioclase. The process of magma mixing is reflected by: (1) ubiquitous sieved-textured plagioclase with complex textural relationships; (2) a large range in plagioclase compositions with reversals and spike patterns in profiles; (3) embayed and internally fractured (thermal shock?) quartz; (4) the rare occurrence of pyroxene coronas on quartz; and (5) textures within biotite suggestive of its incipient breakdown. The lack of mafic enclaves indicates that physico-chemical conditions of the mixing were conducive to homogenization (i.e. chemical diffusion) and a superficially homogeneous rock is now observed. The association of glomeroclasts of crystals originating from both the mafic and felsic end members and a quenched quartz-feldspar matrix indicate that the mixing occurred in an underlying magma chamber.

KEYWORDS: granite, peraluminous, magma mixing, Minastira, Peru.

Introduction

THE Cordillera de Carabaya segment of the Cordillera Oriental of SE Peru (Fig. 1) exposes a range of intrusive and extrusive magmatic suites of Permian to Pliocene age that record the involvement of both mantle and crustal reservoirs (Kontak *et al.*, 1984, 1985, 1990; Clark *et al.*, 1984, 1990*a*; Sandeman *et al.*, 1995). In several districts, field, petrographic and petrochemical relationships strongly suggest that the influx of mantle-derived basic magma contributed to the fusion of the continental crust under conditions in which the 'parental' and 'daughter' magmas could subsequently commingle at shallow depths. For example, Kontak *et al.* (1986) demonstrated that the

[1] Present address: Nova Scotia Department of Natural Resources, P.O. Box 698, Halifax, Nova Scotia, Canada B3J 2T9.

Mineralogical Magazine, December 1997, Vol. 61, pp. 743–764

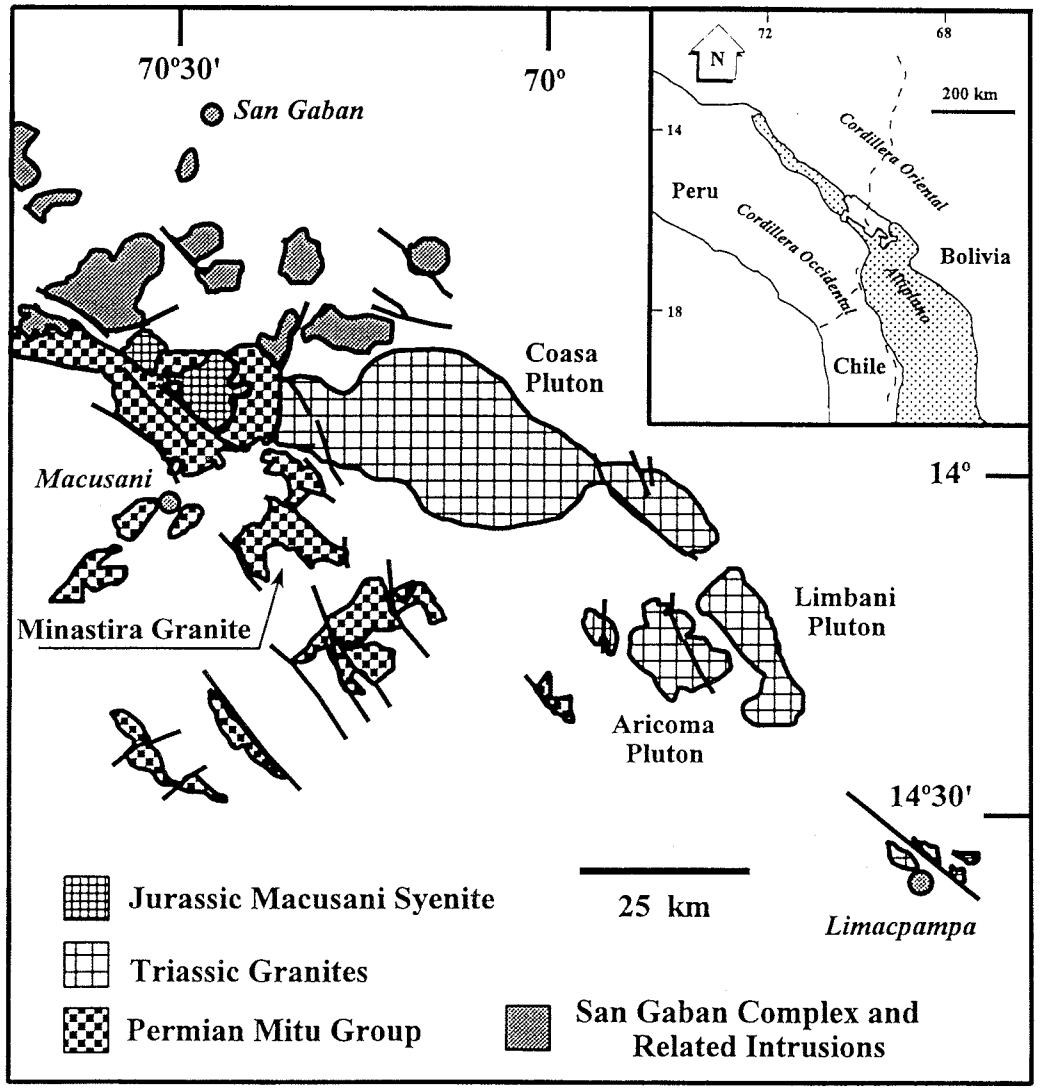

FIG. 1. Location of the study-area (Cordillera de Carabaya) in the Central Andes of Peru with the broad lithotectonic subdivisions shown. Simplified geology shows the distribution of igneous rocks, intrusive and extrusive, in the study area with the area in white mainly underlain by a dominantly Lower Palaeozoic package of metasedimentary rocks. Location of the Minastira granite is indicated by the arrow (note that the size of the intrusion is too small to show at this scale).

c. 25 Ma Cerro Moro Moroni (or Moromoroni) volcanic suite exhibits both mineralogical and chemical evidence for commingling and mixing of K-rich mafic (absarokitic) and highly peraluminous felsic melts, the latter represented by a cross-cutting biotite monzogranite dyke. However, the basic character of the volcanic suite was maintained and the contribution of the felsic melt component to the exposed extrusive rocks was thus minor. Subsequently, work by Sandeman *et al.* (1996*a*,*b*) has shown that this commingling of mafic and felsic melts is widespread throughout the Cordillera de Carabya region of SE Peru, and involved both basaltic and lamprophyric mafic end-members.

Several broadly coeval peraluminous cordierite (± sillimanite)-biotite monzogranite stocks have been delimited within a few km of the Moro Moroni centre (Clark *et al.*, 1983, 1984 Kontak *et al.*, 1987; Kontak and Clark, 1988; Sandeman, 1995), but the role of magma mixing processes in their evolution is unclear. However, a small hypabyssal body of fine-grained granitoid rock in the Minastira district (Fig. 1) is interpreted herein to represent the product of a system of magma mixing where the felsic component was dominant. The subvolcanic setting of this intrusion has permitted the preservation of petrographic evidence of the mechanisms of magma commingling and mixing which would normally not survive either the protracted annealing unavoidable in deeper-seated plutons or the violence of pyroclastic eruption.

Geological setting

The study area is located within the Inner Arc system (Clark *et al.*, 1984, 1990*a*) of the Central Andean orogen, broadly cospatial with the Cordillera Oriental of Peru and Bolivia (Fig. 1). In this region, post-Carboniferous magmatism has been both episodic and extremely varied in nature (Kontak *et al.*, 1984, 1990), contrasting with the quasicontinuous and largely calc-alkaline subduction zone-related magmatism of the Main Arc (e.g. Pitcher *et al.*, 1985, and references therein). The Inner Arc is located at the interface between the Brazilian craton and the Andean orogen (Kontak, 1985), and the magmatic evolution of this narrow lithotectonic domain has been strongly influenced by the gross tectonic relationships between the two geotectonic provinces.

The geological evolution of the Cordillera de Carabaya is reviewed elsewhere (Laubacher, 1978; Kontak, 1985). The oldest-exposed rocks, pelitic and psammitic strata of Ordovician–Devonian age which attain 15 km in thickness, are overlain unconformably by some 3 km of Carboniferous–Lower Permian psammites and limestones and up to 3 km of Permian molasse sediments. Magmatism in the region commenced in the Early Permian (Clark *et al.*, 1990*b*), prior to the initiation of Andean orogenesis in the mid-Triassic, and persisted to at least the Pliocene. The most voluminous igneous rocks are those of the Upper Triassic–Lower Jurassic Carabaya Batholith (Kontak *et al.*, 1985, 1990), which displays evidence of commingling and mixing of melts derived from the mantle and crust. The much younger rocks described herein are representative of the San Rafael intrusive suite, a lithodemic unit of the Upper Oligocene–Lower Miocene Picotani Group, itself part of the Crucero Supergroup (Sandeman, 1995; Sandeman *et al.*, 1996*a,b*).

The Minastira granite (latitude, 14°10′42″″ S; longitude 70°15′31″ W) comprises several small plugs (<100–1000 m^2 in area) hosted by red quartz arenites of the Cretaceous Cotacucho Group (Laubacher, 1978). The contacts are not exposed and no thermal aureole is detectable. Phenocrysts of quartz, translucent alkali feldspar and biotite are evenly distributed in an aphanitic, dark-green matrix. The intrusive rocks appear to be unweathered. Conventional K–Ar dating of unaltered biotite (Kontak *et al.*, 1987) yields an age of 24.2 ± 0.5 Ma, indicating that intrusion occurred in the latest-Oligocene, coeval with eruption of the mafic-to-felsic Picotani Group strata of the Cordillera de Carabaya (Sandeman *et al.*, 1996*a,b*).

Petrography of the Minastira granite

Xenolith

A single inclusion (2 mm) of metasedimentary rock consists of fibrolitic sillimanite, and lesser biotite, plagioclase, spinel and zircon. The absence of a reaction rim about the fragment suggests that it was entrained as the magma approached its level of emplacement. Similar xenoliths have been reported by Injoque *et al.* (1983) to occur in an Upper Miocene subvolcanic intrusion in the Choquene mining district, *c.* 80 km ESE of Minastira (Yamamura, 1991).

Glomeroclasts

Glomeroclasts, of 2–3 mm size and exhibiting granophyric texture, are observable only in thin section. Two types are distinguished: (1) quartz-alkali feldspar-biotite-brown ferromagnesian phase (Fig. 2*a*); and (2)) sieve-textured plagioclase-biotite ± hercynitic spinel ± brown ferromagnesian phase ± apatite (Fig. 2*b*). These mineral phases also occur as individual grains in the granite (see below), but this is the only observed occurrence of spinel of probable magmatic origin in the Minastira rocks. It is emerald-green, fine-grained, euhedral, and occurs as inclusions within plagioclase grains adjacent to the brown ferromagnesian phase. The second type of glomeroclast is distinguished by a granophyric texture (Fig. 2*a*) and arrays of negative-shaped, vapour-rich inclusions in quartz.

Mineralogy of the granite

The intrusive rocks exhibit a mineral assemblage with several unusual, and in part problematic, features, as summarized in Table 1 and illustrated in Figs. 2 and 3.

Quartz phenocrysts (< 1 mm to 5 mm) are either euhedral or embayed, the latter grains transected by fractures disposed in curving arrays paralleling their

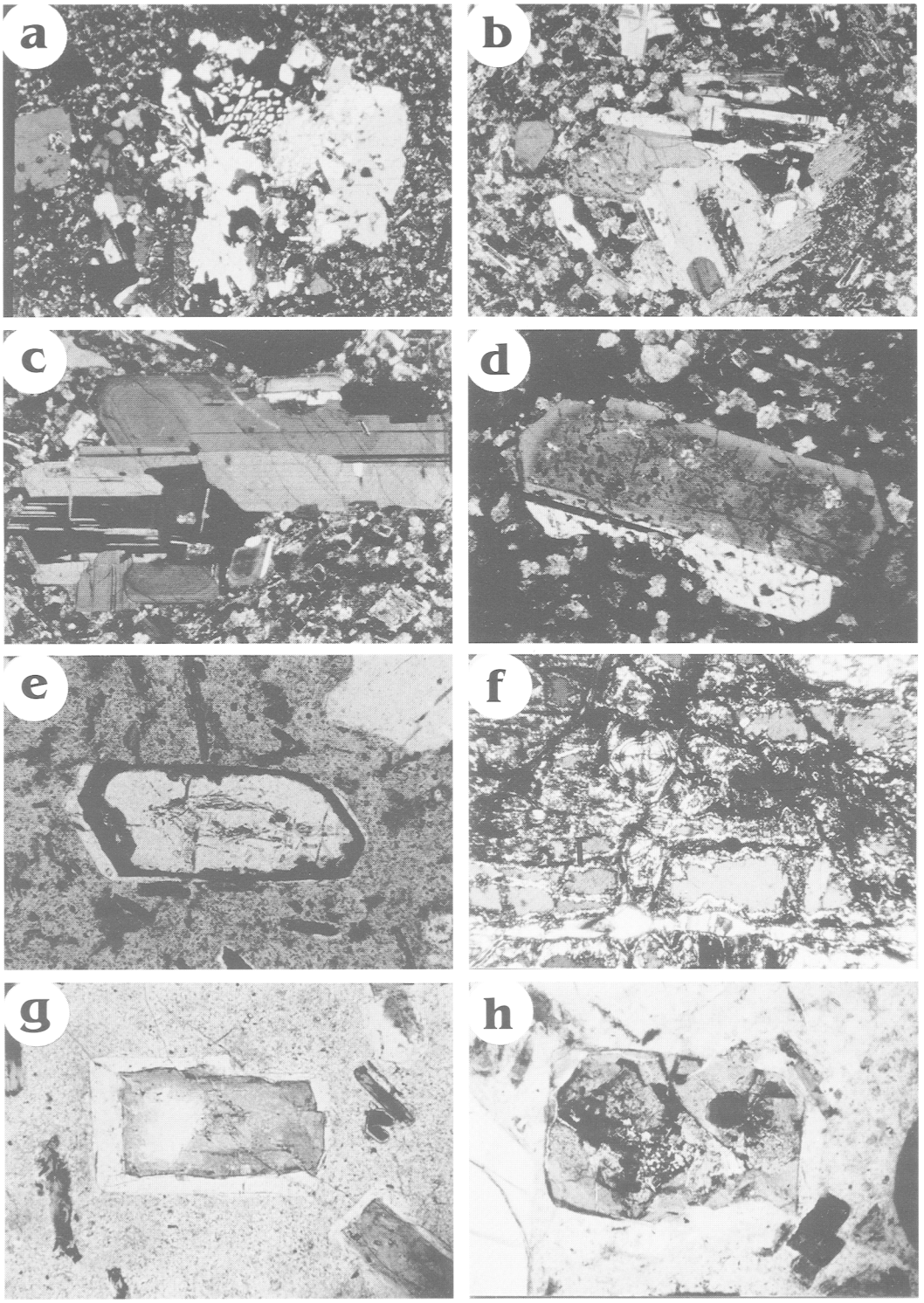
a
b
c
d
e
f
g
h

margins. The fractures are filled with fine-grained, microscopically brown and grey material that is apparently identical to the matrix phases of the rock. Narrow brownish, crystalline rims surround some quartz grains and are probably pyroxene (cf. Sato, 1975; Kontak *et al.*, 1986; Stimac and Pearce, 1992). The quartz phenocrysts host glass-bearing and fluid inclusions, bodies of a brown, apparently secondary alteration phase with or without a feldspar rim, zircon euhedra lacking corroded cores, and flakes of biotite. The glass-bearing inclusions are diverse, and include examples: (1) with rectangular outlines, containing microlites of unknown composition (feldspar?) in an isotropic medium, and with narrow border-zones of a crystalline material with undulose extinction and incorporating a fine-grained opaque phase; (2) with rectangular shapes but consisting of glass, a vapour bubble and a microlite; (3) comprising green and brown birefringent phases + glass + an opaque mineral ± a vapour bubble; and (4) containing an opaque phase and glass in variable proportions. Other, probably allied inclusions are made up of completely crystallized, feather-textured and in part spherulitic material of feldspathic composition (qualitative electron microprobe data) and minor amounts of equant opaque minerals. Semi-quantitative electron-probe microanalysis of several opaque phases in inclusions of types 1 and 3 reveals the presence of both an Fe-Ti oxide mineral containing minor Cr (< 1 wt.% Cr_2O_3) and a Cu-Fe sulphide with optical properties and approximate composition conforming to those of chalcopyrite.

Biotite (2–3 mm) occurs as brown microphenocrysts with variable absorption (Fig. 2*b,e*) that are incipiently altered to chlorite and invariably contain numerous fine-grained inclusions of ilmenite and of unknown, probably secondary, phases occurring either at the margins of the grains or along cleavage traces. This latter texture is similar to that described by Nixon (1988) and Stimac and Pearce (1992), and attributed to the breakdown of biotite due to dehydration above its stability field. A reddish and transparent phase is tentatively identified as rutile. Biotite is generally free of other inclusions, but some grains contain: (1) coarse apatite crystals, some projecting into the matrix (rare); (2) plagioclase laths (very rare); and (3) bodies of an unidentified brown phase that appears similar to that occurring in the matrix of the rock (see below). Biotite rarely occurs as inclusions in plagioclase, where it is finer-grained but again contains the aforementioned opaque and related phases. Where several biotite grains are hosted by a single plagioclase crystal, they are concentrically arranged about its core.

Plagioclase (< 1 mm to 6–8 mm) occurs both as single grains of variable habit (Fig. 2*c,d,e*) and as a constituent of glomeroclasts (Fig. 2*a,b*). The coarser grains are generally euhedral-to-subhedral but some are broken; in contrast, the finer grains are euhedral. In detail, the plagioclase is very heterogeneous in form, including: (1) simple grains that are normally zoned and contain few inclusions (Fig. 2*c*); (2) euhedral, zoned grains exhibiting varying amounts of a brown ferromagnesian phase (Fig. 2*e*; up to 90% of the finer-grained plagioclase may be replaced by this phase: see below) (3) coarse grains with pervasive or, more widely, marginal sieve texture (Fig. 2*d*); (4) rare grains with zonally-concentrated inclusions of sillimanite, biotite, zircon and the brown ferromagnesian phase (Fig. 2*e*); and (5) grains with 30–50 μm, vapour-dominated, fluid inclusions of very irregular shape (aspect ratios, 25–50:1).

Sanidine, a minor constituent, forms 2–9 mm grains of euhedral-to-anhedral habit, most commonly microphenocrystic, and some with biotite, glass and vapour-rich fluid inclusions. The grains are either

FIG. 2. Transmitted-light photomicrographs of the Minastira granite. All photos taken in crossed nicols except for e, g and h. (*a*) Glomeroclast showing granophyric texture. Note that the feldspars are unaltered and do not exhibit sieve textures. Width of field is 1 cm. (*b*) Glomeroclast consisting of plagioclase and biotite. The plagioclase has sieve textures, is cored by a brown ferromagnesian phase (see text), and is strongly zoned. Width of field is 1 cm. (*c*) Euhedral, strongly-zoned plagioclase grain clear of both mineral and melt inclusions, and alteration phases. Width of photo is 6 mm. (*d*) Strongly-zoned, subhedral plagioclase grain with sieve-textured core; note that the overgrowth border is free of melt inclusions. Width of photo is 1.3 mm. (*e*) Euhedral plagioclase with oriented sillimanite grains outlining the core and a zone near the grain margin containing the brown ferromagnesian phase. The grain in the upper right is partially resorbed quartz and the dark, acicular grains in the matrix are biotite. Width of photo is 5 mm. (*f*) Alkali feldspar grain showing incipient stages of conversion to unidentified material with perlitic-like texture (possibly internal melt) along fractures traversing the grain. This is the only grain in which this phenomenon was observed. Width of photo is 5 mm. (*g* and *h*) Subhedral to euhedral grains of a brown to greenish-brown ferromagnesian phase illustrating some of the unusual textural relationships. In Fig. 2*g* a plagioclase mantle is seen surrounding two grains of the brown phase (centre and lower right of photo) whereas in Fig. 2*h* variations in colour occur within the alteration phase (not seen in black and white) and additional phases are locally developed (core area of grain). Width of photos are 0.67 mm (*g*) and 1.3 mm (*h*).

TABLE 1. Summary of mineralogy of Minastira Granite, SE Peru

	Quartz	Biotite	Plagioclase	Sanidine
Size	<1 to 5 mm	2–3 mm	<1 to 6–8 mm	2–8 mm
Shape	euhedral-to-embayed	equant, euhedral	subhedral-to-euhedral	euhedral-to-anhedral
Internal fractures	numerous curvilinear fractures; embayed	alteration/reaction along cleavage	sieve textures; complex zoning	embayed; melt features with perlitic textures
Reaction rim	brown crystalline material (pyroxene?)		some grains bordered by brown phase	red-brown phase at margins
Inclusions	melt; fluid inclusions; biotite-zircon; brown phase	ilmenite; rutile(?) apatite; plagioclase; brown phase	melt inclusions; apatite; sillimanite; biotite; zircon; brown phase; fluid inclusions	biotite; melt inclusions; fluid inclusions

	Apatite	Brown phase
Size		<4–5 mm
Shape	subhedral-to-euhedral	anhedral-to-subhedral; rectangular
Internal features	lamellae of sagenite texture	
Reaction rim		may be rimmed by plagioclase
Inclusions	zircon; monazite; apatite; sillimanite; unknown phases	

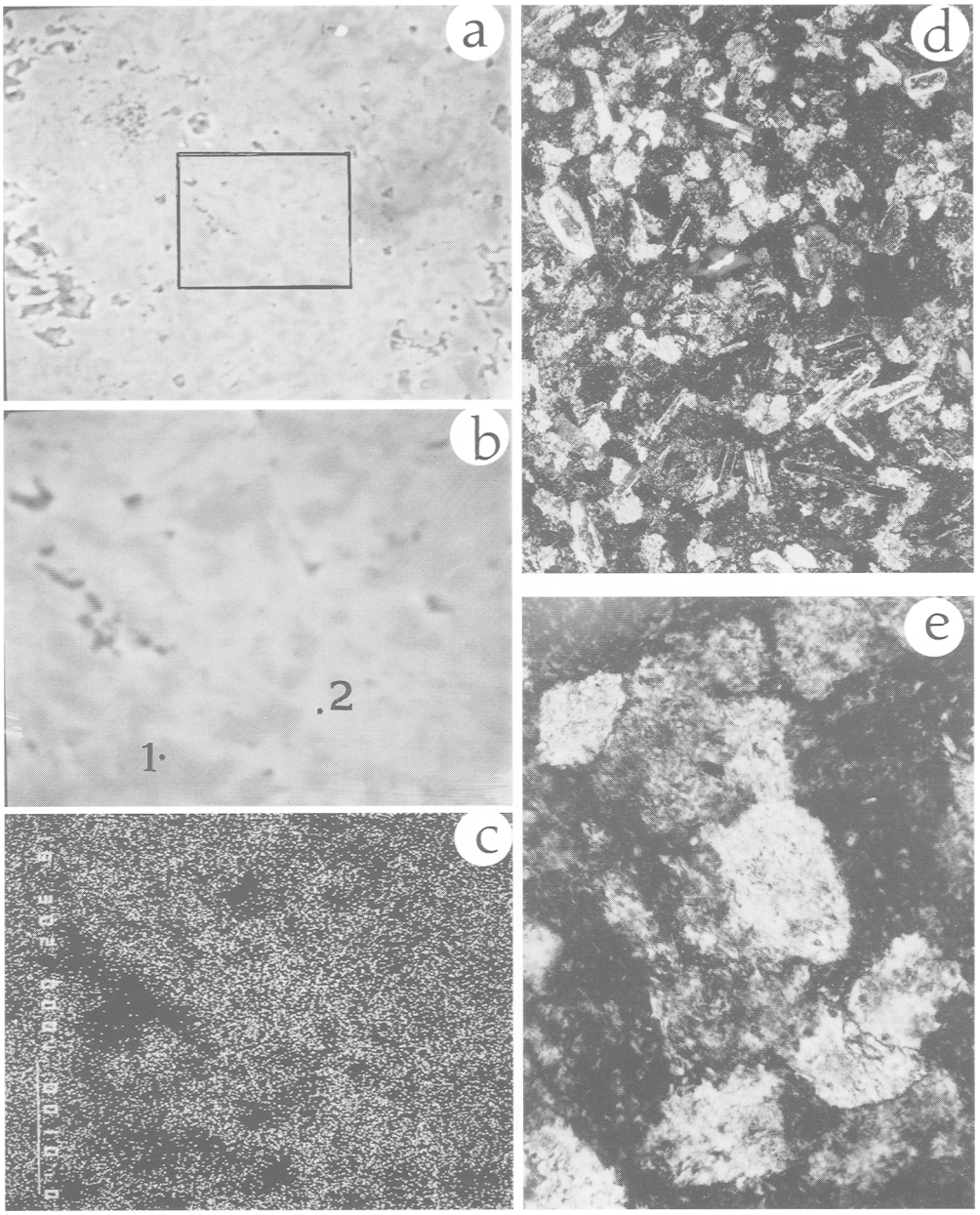

FIG. 3. Back-scattered electron (BSE) images and photomicrographs of matrix material in the Minastira granite. (*a*) and (*b*) are BSE images illustrating the two components of the matrix. The dark material is silica-rich (i.e. 94–99 wt.% SiO_2) whereas the pale is enriched in silica, alkalis and alumina. Note that Fig. 3*b* is an enlargement of the boxed area in Fig. 3*a*. Points 1 and 2 in Fig. 3*b* refer to analyses given in Table 3. (*c*) X-ray image for the area shown in Fig. 3*b* illustrating the distribution of K which essentially matches the paler areas. The areas that are depleted in K correspond to the silica-rich areas in Fig. 3*b* (i.e. dark patches). Scale bar is 100 μm. (*d*) Photomicrograph (crossed nicols) of the matrix illustrating the generally hypidiomorphic granular texture (long dimension about 2.6 mm) (*e*) Photomicrograph (crossed nicols) of the matrix showing its typical texture (long dimension about 0.67 mm.).

embayed or rimmed by fine-grained, unidentified, reddish-brown or colourless phases. Some coarse sanidine grains have ragged interiors with volumes of perlitic-textured material (Fig. 2*f*).

Apatite, an abundant constituent, occurs as coarse, generally euhedral grains in the matrix and more rarely in biotite and plagioclase phenocrysts. Fine, dark lamellae that define crystallographic planes, and reminiscent of 'sagenite', are commonly developed in the margins of the apatite grains and in some cases extend into their cores. Other apatites contain numerous euhedral mineral inclusions, crudely defining concentric patterns and including zircon, monazite, rare sillimanite and at least three unknown phases. Some apatite grains enclose a variety of melt-derived inclusions, including: (1) undevitrified glass-vapour-crystal systems, in which the crystals (1–3 phases) include an opaque phase and two birefringent minerals, one equant and the other acicular; (2) bodies of feldspathic material with a 'spinifex-like' texture similar to that observed in inclusions in quartz (see above), together with grains of a red, probably Fe-bearing, mineral; and (3) undevitrified glass lacking crystalline phases.

One of the most common phenocrystic components is a *brown to greenish-brown ferromagnesian phase* exhibiting a variety of textures. It displays rectangular, cubic, pentagonal and hexagonal sections, varies in size from microlitic to phenocrystic (4–5 mm), ranges from brown to olive-green, some grains being colour-zoned, and is commonly mantled by a euhedral rim of zoned plagioclase (Fig. 2*e,g,h*). In high magnification radial, cuspate and colloform textures similar to clay minerals are observed. This phase also occurs coring plagioclase, within biotite and rarely in apatite. Although no single mineral can be reconciled with the range of morphology, some grains resemble pinnitized cordierite.

The matrix of the rock consists of microlites of most of the above mentioned constituents embedded in an equigranular quartz-alkali feldspar intergrowth (Fig. 3) which, in high magnification back-scattered electron (BSE) imaging, reveals crudely feathery textures (Fig. 3*a,b*). The latter textures are very similar to those figured in London *et al.* (1993) and generated through devitrification of H_2O-saturated, subaluminous haplogranite glasses.

In summary, the petrographic features of the Minastira granite clearly record an association of phases which are not entirely in mutual equilibrium and have either individually or collectively undergone a complex history. The presence of such features as embayed and corroded quartz grains with pyroxene rims, sieve-textured plagioclase, and embayed sanidine with internal melting features is, by analogy to other petrological settings, strongly suggestive of magma mixing.

Geochemistry

Analytical procedures

Analyses of whole-rock samples of the Minastira granite and a biotite separate have been determined (Kontak, 1985) using a Siemens Model VRS X-ray Fluorescence Spectrometer on fused (major elements) and unfused (trace elements: Rb, Sr, Ba, Nb, V, Cr, Zr, Y, Sn) powders. Additional trace elements (Cu, Pb, Zn, Ni) were analysed on an Instrumentation Laboratory Model 251 Atomic Absorption Spectrophotometer, while ferrous iron contents were determined by titration. A single whole-rock sample was analysed for *REE* using the thin-film X-ray fluorescence method of Fryer (1977). The compositions of biotite, feldspars, apatite and oxides, as well as of the unknown alteration (?) phases and the rock matrix, were determined using a JEOL 733 Superprobe, using a combined wave-length- and energy-dispersive analytical technique and the following operating conditions: accelerating voltage 15 kV, a probe current of about 5 nÅ and a beam diameter of about 1–2 μm (defocussed to 5 μm for feldspar and matrix). Data reduction was carried out with the ZAF soft-ware program.

Whole-rock chemistry

Analyses of two granite samples are recorded in Table 2 and are compared to analyses of the coeval, strongly peraluminous, cordierite-bearing San Rafael granite (Palma, 1981; Kontak, 1985). The two samples of the Minastira granite are similar in composition, with the exception of TiO_2 and a granodioritic composition is defined (66 wt.% SiO_2). The rock is markedly peraluminous (A/CNK=1.56 and 1.87), strongly reduced (Fe_2O_3/FeO = 0.83 and 1.16) and K-rich (K_2O/Na_2O = 1.55 and 1.86); the cafemic components, MgO, CaO, MnO and TiO_2 are depleted. The P_2O_5 content is similar to that of the San Rafael granite and other peraluminous granites of similar SiO_2 content (e.g. London, 1992; Pichavant *et al.*, 1992).

Trace element contents for the two samples (avg. in ppm) are as follows: Rb (341), Ba (725), Sr (153), Zr (150), Sn (13), Nb (12), V (58), Ni (13), Cu (12), Pb (56) and Zn (83); these abundances compare well with those in the average S-type granite of the Lachlan Fold Belt of Australia (White and Chappell, 1983). Compared to the San Rafael granite, the Minastira intrusion is enriched in Nb, depleted in Ba, Sr and Zr, comparable with respect to V, Rb and Sn (Table 2), and in terms of element ratios has higher Rb/Sr, lower K/Rb and comparable Ba/Sr. There is no enrichment in metalliferous elements such as Cu, Pb, Zn or Sn.

The chondrite-normalized *REE* pattern for the granite is compared in Fig. 4 to the field (n = 15)

TABLE 2. Whole-rock geochemistry for Oligocene–Miocene granites, SE Peru

Material Sample	Granite CC-282	Granite CC-283	Biotite CC-284	Granite CC-406	Granite CC-408
SiO_2	66.91	66.42	35.2	66.4	66.5
TiO_2	0.14	0.43	3.69	0.48	0.49
Al_2O_3	16.2	15.33	16.98	16.1	15.91
Fe_2O_3	1.18	1.38	1.1	2.62	3.27
FeO	1.42	1.18	17.5	NA	NA
MnO	0.03	0.04	0.11	0.07	0.1
MgO	1.48	1.79	10.84	1.55	1.44
CaO	1.49	1.07	0.33	1.34	0.78
Na_2O	3.03	2.58	0.62	3.41	2.71
K_2O	4.72	4.82	8.52	4.59	5.64
P_2O_5	0.21	0.23	0.12	0.21	0.21
Trace elements (ppm)					
Rb	338	344	787	310	358
Sr	176	130	16	294	209
Ba	701	751	1868	1194	911
Nb	13	12	79	7	8
Zr	155	145	194	186	187
V	62	54	398	63	57
Cr	NA	NA	372	48	48
Ni	14	11	NA	NA	NA
Cu	11	12	NA	NA	NA
Pb	63	49	NA	NA	NA
Zn	87	80	NA	NA	NA
Sn	11	16	NA	20	4
Rb/Sr	1.92	2.64	–	0.05	1.71
Ba/Sr	3.98	5.77	–	4.06	4.35
K/Rb	116	116	–	122	130
A/CNK	1.56	1.87	–	1.24	1.33

Samples CC-282, 283 and 284 from Minastira;
Samples CC-406 and 408 from San Rafael

delimited by other peraluminous Oligocene–Miocene granitoids of SE Peru, including a single analysis of an exceptionally fresh granodiorite (CC-406) from San Rafael. The latter sample is from the upper, chilled part of the San Rafael intrusion (Kontak and Clark, 1988) and is considered to be representative of an early and relatively undifferentiated facies of that pluton. The *REE* pattern for the Minastira granite is strongly fractionated, with $(La/Yb)_N = 69$ and a strong negative Eu anomaly ($Eu/Eu^* = 0.2$). The latter feature is intriguing because of the elevated Ba and Sr contents, possibly inherited from magma mixing (see below), and the low percent of feldspar in the granite, thus inheritance due to mixing may be indicated. The ΣREE is notably depleted compared to that in the San Rafael and other Oligocene-Miocene granitoids of SE Peru, although the chondritic patterns are similar overall for all samples and are typical of peraluminous suites (e.g. Muecke and Clarke, 1981).

Matrix composition

The bulk composition of the matrix of the Minastira granite may represent the magma in equilibrium with the phenocryst assemblage (i.e. rim phases). Because of its very fine-grained nature and the occurrence of distinct domains (Fig. 3*a,b*) it was necessary to use BSE imaging to locate the electron beam prior to microprobe analysis; a BSE image for potassium (Fig. 3*c*) illustrates the markedly varying content of that element. Representative matrix compositions are given in Table 3. The data (n = 59; Fig. 5) indicate that there are large ranges in SiO_2 (66 to 99 wt.%), Al_2O_3 (below detection (ND) to 19 wt.%), K_2O (ND

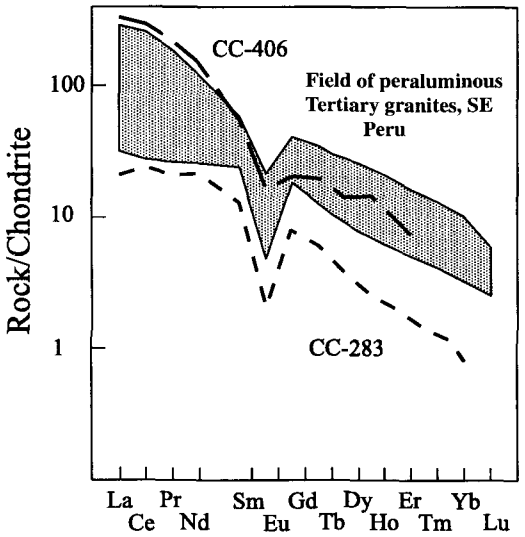

FIG. 4. Chondrite-normalized plot for granites of the Cordillera de Carabaya region of SE Peru. The Minastira granite is represented by CC-283, and the San Rafael granite by CC-406 (see text for discussion). The compositional range for the peraluminous Miocene–Pliocene granites (n = 15) in the study area is delimited (Kontak and Clark, 1988).

to 10 wt.%) and Na_2O (ND to 3.5 wt.%), with minor to trace amounts of CaO, FeO and MgO. In addition, TiO_2 is < 0.1 wt.%, BaO is generally < 0.1 wt.% but in some areas attains 0.3 wt.%, P_2O_5 is $\leqslant$ 0.3 wt.% and F and Cl were not detected (detection limit *c.* 0.1 wt.%). The lack of F is surprising in view of its elevated content in biotite (see below) and the felsic nature of the matrix. Strong correlations are evident between SiO_2 and the major elements K, Na and Al (but note the convergence problem at high SiO_2 values), although there is a notable scatter for K and Na in the least silicic areas. In contrast, Ca correlates relatively poorly with SiO_2 compared to the former elements, in part due to contents approaching limits of detection.

The matrix is strongly potassic with K_2O/Na_2O ranging between 1.5 and 4.5 (Fig. 5); these values compare with the values of 1.55 and 1.86 for the whole-rock analyses (Table 2). In the K_2O+Na_2O vs. SiO_2 plot, the trend extends to a composition, about 65 wt.% SiO_2 and 14 wt.% alkalis, approximating that of alkali feldspar, although the analyses do not conform to stoichiometric alkali feldspar.

Finally, we note that the most siliceous domains (i.e. >92 wt.% SiO_2) of the matrix contain substantial Al_2O_3 and alkalis. Detailed electron microprobing in such areas (10–15 μm apart) reveals a variation of up to 3–4 wt.% SiO_2; comparable variability was found for the relatively SiO_2-poor areas.

Mineral chemistry

Sanidine has a uniform composition (Or_{67-76}: Table 4 and Fig. 6), the maximum zonation detectable in a single grain being 5–6 mole % Or. In some grains an increase in Ba content from cores (e.g. 0.21 wt.% BaO) to rims (0.48 wt.%) is noted. Cavities lined with anhedral-to-subhedral alkali feldspar grains have been observed in several sieve-

TABLE 3. Representative analyses of matrix material, Minastira granite, SE Peru

Point	3-21	3-30	3-15	3-13	3-6	2-44	2-8	1-52	3-4	1	2
SiO_2	99.38	98.39	95.52	89.43	81.52	76.42	79.87	73.74	67.97	95.08	73.68
TiO_2	0.07	0.08	ND	ND	ND	0.09	ND	ND	ND	0.07	0.10
Al_2O_3	1.03	2.02	3.05	5.81	10.34	14.41	12.73	15.13	18.76	3.46	15.61
FeO	0.15	0.11	ND	0.11	0.17	0.08	ND	0.11	0.22	0.11	0.13
MnO	ND	ND	ND	ND	ND	ND	0.15	ND	ND	ND	ND
MgO	ND	0.06	ND	0.14	ND	ND	ND	ND	ND	0.09	0.06
CaO	ND	ND	ND	0.09	0.37	0.54	0.29	0.21	0.37	0.09	0.18
Na_2O	ND	0.22	0.39	0.94	1.94	2.53	2.41	2.37	2.81	0.39	2.36
K_2O	ND	0.39	1.27	2.45	4.42	6.54	6.32	8.43	9.45	0.03	8.42
P_2O_5	ND	0.13	0.23	ND	ND	0.21	ND	ND	0.26	ND	0.30
BaO	ND	ND	ND	ND	ND	ND	ND	0.24	0.28	ND	ND
Total	100.63	101.40	100.46	98.97	98.76	100.82	101.77	100.23	100.12	100.22	100.84

Note: Points 1 and 2 refer to the BSE image in Figure 3.

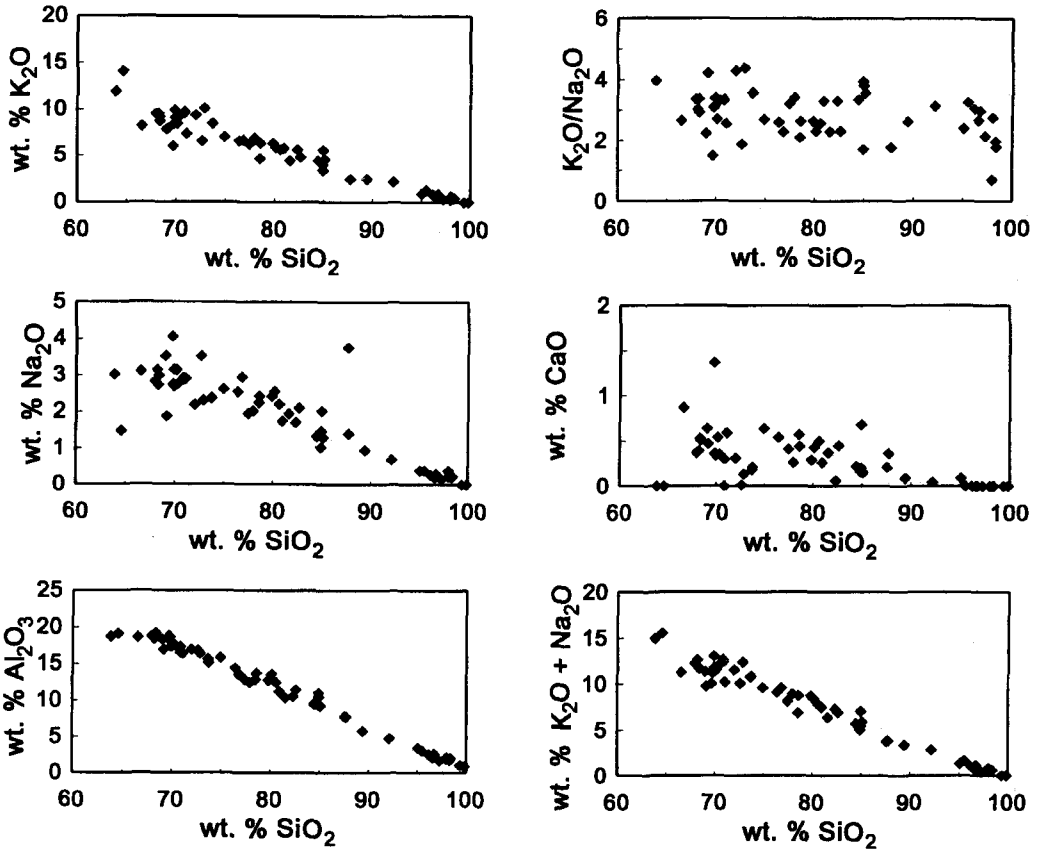

FIG. 5. Binary element variation diagrams for matrix material of the Minastira granite. As discussed in the text, the increase in apparent correlation towards higher silica values is a result of convergence.

textured plagioclase grains and range in composition from $Or_{58}Ab_{40}An_2$ to $Or_{65}Ab_{35}$ (Fig. 6); thus they are more sodic than the microphenocrystic sanidine. A single grain of alkali feldspar included in biotite has a composition of $Or_{85}Ab_{15}$, with 1.32 wt.% BaO.

Plagioclase exhibits a large range in bulk composition (Table 4; Fig. 6, 7) with limiting compositions of $An_{58}Ab_{38}Or_4$ and $An_{20}Ab_{75}Or_5$; we emphasize the high potassium contents (cf. Deer *et al.*, 1966). The compositions of the rims of plagioclase grains are consistently in the range An_{27} to An_{31}, and oscillatory zoning of some 4–5 mole % An occurs. An analysis (An_{15}) that diverges from this trend was for a grain adjacent to a cavity infilled by quartz and sanidine. Subdivision of the compositional data in terms of the plagioclase morphotypes (Table 4; Fig. 7) reveals no systematic trends, but shows that: (1) overgrowths on the brown ferromagnesian phase are An_{30-48}; (2) sieve-textured rims of phenocrysts are An_{28-44}; (3) patches intergrown with or overgrown by the brown ferromagnesian phase have compositions of An_{35-55}; (4) the matrix plagioclase, An_{33-40}, is not the most sodic in composition; and (5) microphenocrysts range from An_{20} to An_{56} with an apparent gap at An_{40-50}. Zoning profiles for representative grains (Fig. 8) indicate that at least in some cases the sieve-textured plagioclase is more calcic than clear areas.

Biotite (Table 5; Fig. 9) is annitic in composition, more than 90% of the samples falling in the compositional range Fe/(Fe+Mg) = 0.45 ± 0.05. MgO varies from 10.5 to 14.8 wt.%, TiO_2 from 2.5 to 4.6 wt.% and Al_2O_3 from 15 to 18.7 wt.% (Fig. 9,*b,c*). Many of the grains incorporate abundant, fine-grained, opaque domains, but no compositional differences were detected in microprobe analyses of these areas *vs.* clear areas within biotite. A single analysis of a biotite separate (Table 2) compares favourably with the electron microprobe data, except for lower MgO and K_2O contents which

TABLE 4. Representative analyses of feldspars, Minastira granite, SE Peru

Phase	K-feldspar	K-feldspar	K-feldspar	Plagioclase	Plagioclase	Plagioclase	Plagioclase
Point	1-3	1-4	2-38	1-8M	1-9C	1-14C	1-60C
SiO_2	66.95	67.35	65.87	62.22	62.32	58.54	56.00
Al_2O_3	19.04	19.00	18.58	24.59	24.57	27.08	28.75
CaO	0.25	0.07	0.11	6.26	6.31	9.28	11.34
Na_2O	3.44	2.79	2.45	6.79	7.05	5.59	4.85
K_2O	11.13	10.97	12.12	0.79	0.81	0.46	0.35
BaO	0.48	0.21	0.26	ND	ND	ND	ND
Total	101.29	100.59	99.39	100.65	101.65	100.95	101.29
An	1.6	0.0	2.0	32.1	31.3	46.6	55.2
Ab	31.0	29.7	23.2	62.6	63.5	50.8	42.2
Or	67.2	70.2	75.8	5.2	5.0	2.5	2.4

Phase	Feldspar	Feldspar	Plagioclase	Plagioclase	Plagioclase	Plagioclase	Plagioclase
Point	3-23I	3-28	3-41C	3-42R	3-62Ralt	3-69Ralt	3-63Calt
SiO_2	67.16	67.19	62.71	59.88	58.82	60.95	60.54
Al_2O_3	20.56	19.73	24.41	26.18	26.99	25.29	25.83
CaO	1.78	1.32	6.13	7.81	9.03	6.88	7.49
Na_2O	5.02	3.48	6.44	5.85	5.39	6.12	6.09
K_2O	5.19	6.12	0.91	0.54	0.43	0.72	0.66
BaO	ND	0.29	ND	ND	0.13	ND	0.25
Total	99.71	98.13	100.60	100.26	100.79	99.96	100.86
An	10.9	9.0	32.4	40.7	46.4	36.6	38.5
Ab	52.9	42.2	62.1	55.7	50.8	58.9	56.9
Or	36.2	48.8	5.5	4.6	2.8	4.5	4.6

Note: M = matrix; R = rim, C = core; alt = alteration; I = inclusion in K-feldspar

may reflect limited chloritization. The Fe_2O_3/FeO ratio is very low (0.06), consistent with similarly low ratios for the whole-rocks and other biotites from SE Peruvian granites (Kontak, 1985; Kontak *et al.*, 1984; Kontak and Clark, 1988); in the Fe^{2+}-Fe^{3+}-Mg diagram of Ishihara (1977) the data plot along the QFM buffer.

The biotite is distinguished from biotites in peraluminous granites in the region by its high Al_2O_3 and MgO contents (Fig. 9). Analytical data, summarized in Fig. 9, show that although there is a general trend of increasing fluorine with decreasing Fe/(Fe+Mg), exemplifying the Fe-avoidance principle (Bailey, 1984), there is overall a large variation in F content [below the limit of detection (*c.* 0.1 wt.%) to 4.5%]. This diagram also illustrates the intra-grain variation in both major element [e.g. Fe/(Fe+Mg)] and F contents. In contrast to the wide range observed for F, the Cl contents are uniformly low at *c.* 0.15 wt.% (Table 5). It is of interest that a biotite enclosed by quartz is the most Mg-rich, but contains negligible F (Fig. 9*d*).

The trace element chemistry of the biotite separate is given in Table 2. Relative to micas in other peraluminous granites in this area, the Minastira sample is enriched in Ba and depleted in Rb. The enrichment in Ba is in conformity with its more magnesian composition (Fig. 9*a*) and is compatible with some Ba enrichment in the feldspars noted above.

Apatite (Table 6) is F-rich (1.7 to 2.8 wt.%), with <0.5 wt.% Cl, minor Fe (0.5 to 1.5 wt.% FeO), and traces of Mn (to 0.4 wt.% MnO) and Na (to 0.25 wt.% Na_2O). No zonation has been detected within grains and there is no compositional variation that can be related to morphology or to the presence of inclusions. An analysis of an apatite included within a coarser grain of this mineral revealed no difference in composition.

Electron microprobe data for the *brown to greenish-brown ferromagnesian phase* are summarized in the

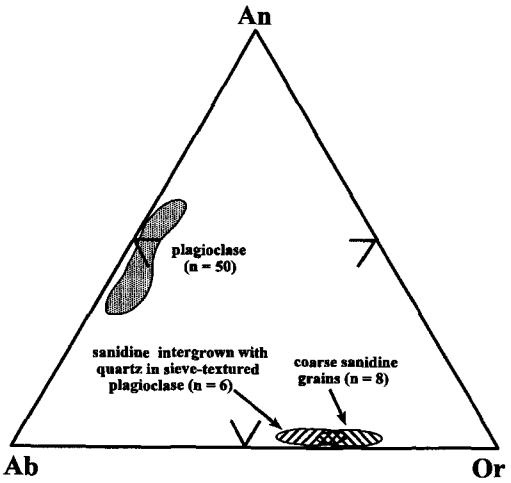

FIG. 6. Ternary plot for feldspar compositional data from the Minastira granite. Not included in this diagram are compositional data from probe traverses of plagioclase shown in Fig. 7.

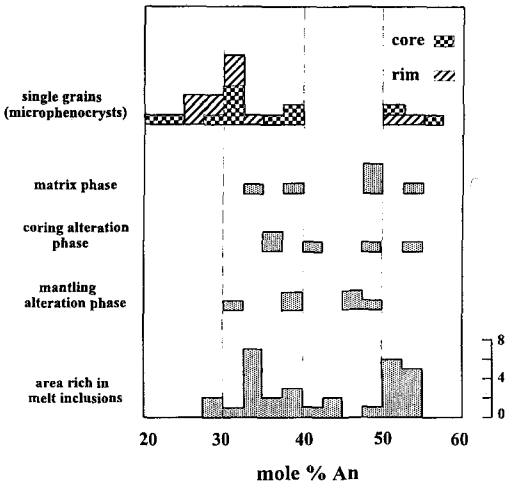

FIG. 7. Histograms summarizing the compositional data (in mole % An) for different textural varieties of plagioclase discussed in the text. Significantly the matrix plagioclase grains are generally more calcic than isolated microphenocrysts.

form of binary element plots for the major oxides, which include SiO_2, FeO, MgO and Al_2O_3 (Fig. 10); representative analyses are given in Table 7. The data have been subdivided on the basis of mode of occurrence, namely: (1) within minerals such as plagioclase, biotite and apatite, (2) as small euhedral grains in the matrix, and (3) as large grains of zoned nature (i.e. with different shades of green and brown). The data reveal a broad range in chemistry with both FeO and MgO varying by 10–12 wt.%, SiO_2 by about 20% and Al_2O_3 by 10%. The totals are low, 83 to 92 wt.%, indicating the presence of water, given that neither F nor Cl was detected in microprobe analysis. With respect to the nature of this material the following points are germane: (1) most analyses reveal an FeO:MgO ratio of 1:1 to 1:4 despite the large range in the absolute abundances of these elements. However, the FeO:MgO ratio increases at elevated content values of MgO with a marked break at 7 wt.% MgO; (2) in most types of occurrence, the FeO:MgO ratio is consistent, although with some exceptions (*e.g.*, matrix grains) the absolute abundance of these elements varies. Thus, a chemical zonation which is consistent with colour variations is presumed to be present within grains; and (3) there is a systematic decrease of the ferromagnesian elements with increasing SiO_2, whereas Al_2O_3 remains fairly constant. Thus, the dominant elemental exchange is (Fe + Mg) $\rightleftharpoons$ Si.

Identification of the ferromagnesian phase remains uncertain, but a tentative interpretation is offered. In Fig. 10 cordierite analyses from a variety of peraluminous felsic suites, both intrusive and extrusive, are plotted for comparative purposes and there is generally a good correlation, the exception being for Mg-enriched cordierites from andesitic volcanics in Martinique (Maury *et al.*, 1985). From this comparison plot we can infer that the Fe-depleted

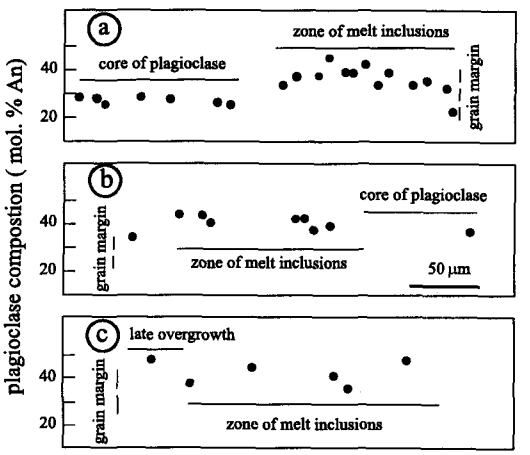

FIG. 8. Partial core-rim profiles of sieve-textured plagioclase grains from the Minastira granite. Note that the distance to the grain margins in profiles 8*b* and 8*c* is greater than indicated with the scale. The indicated scale of 50 μm applies to all three profiles.

TABLE 5. Representative analyses of biotite, Minastira granite, SE Peru

Grain	1	1	2	2	3	3	4	5	6	6
Point	3-3	3-32	3-39	3-40	3-44	3-45	3-67	3-77	3-65	3-66
SiO_2	37.46	37.48	33.92	36.11	36.77	36.70	36.77	36.10	35.87	31.82
TiO_2	3.75	3.99	3.12	3.42	3.17	3.13	3.01	3.82	3.28	2.77
Al_2O_3	15.21	15.39	15.75	16.69	16.36	16.76	16.86	15.33	16.89	19.94
FeO	16.47	14.70	24.30	19.03	18.48	17.98	18.52	14.81	16.74	21.46
MnO	ND	0.28	0.09	0.12	ND	0.12	0.11	0.19	ND	ND
MgO	14.04	14.78	11.09	12.23	12.08	12.00	12.14	14.77	13.41	12.23
CaO	0.00	0.00	0.00	0.00	0.00	0.06	0.00	0.00	0.00	0.00
Na_2O	0.64	0.77	0.57	0.64	0.61	0.61	0.62	0.69	0.56	0.80
K_2O	8.89	8.94	8.50	9.33	9.16	8.96	9.19	9.24	9.19	7.86
BaO	0.64	0.52	0.00	0.00	0.39	0.47	0.51	0.00	0.00	0.20
F	4.35	4.34	1.84	2.80	0.58	0.13	1.10	0.00	3.96	3.16
Cl	0.14	0.15	0.13	0.15	0.15	0.12	0.18	0.11	0.12	0.15
Total	1.59	101.34	99.31	100.52	97.75	97.04	99.63	96.06	100.02	100.39
F, Cl=O	1.86	1.86	0.79	1.20	0.27	0.07	0.50	0.02	1.69	1.36
Total	99.73	99.48	98.52	99.32	97.48	96.97	99.13	96.04	98.33	99.03
Structural Formulae (11 Oxygens)										
Si	2.772	2.761	2.596	2.684	2.739	2.728	2.728	2.750	2.684	2.409
Al(iv)	1.227	1.239	1.403	1.316	1.261	1.272	1.272	1.250	1.316	1.591
Al(vi)	0.093	0.092	0.016	0.147	0.180	0.202	1.474	0.092	0.169	0.191
Ti	0.209	0.220	0.176	0.187	0.176	0.176	0.165	0.200	0.187	0.154
Fe	1.023	0.902	1.562	1.188	1.155	1.122	1.144	0.913	1.045	1.364
Mn	0.000	0.022	0.011	0.011	0.000	0.011	0.011	0.011	0.000	0.000
Mg	1.551	1.617	1.265	1.353	1.342	1.331	1.342	1.628	1.960	1.320
Ca	0.000	0.000	0.000	0.000	0.022	0.011	0.000	0.000	0.000	0.000
Na	0.088	0.110	0.088	0.088	0.088	0.088	0.088	0.099	0.077	0.121
K	0.836	0.836	0.836	0.880	0.869	0.847	0.819	0.869	0.880	0.759
Ba	0.000	0.011	0.000	0.000	0.011	0.011	0.011	0.000	0.000	0.011
F	1.012	1.067	0.451	0.660	0.143	0.033	0.253	0.000	0.935	0.759
Cl	0.022	0.022	0.022	0.022	0.022	0.011	0.022	0.011	0.011	0.022

samples with FeO:MgO of 1:2 to 1:4 may represent loss of Fe during alteration or represent another distinct phase. In Fig. 11, a ternary plot (wt. %) of SiO_2-Al_2O_3-(FeO+MgO), the ferromagnesian phase is compared to compositions of a variety of potential primary and secondary minerals, including cordierite, osumulite, pinnite and vermiculite. In addition, we note that the range of analyses of the unknown phase(s) indicates a chemistry comparable to smectite-, vermiculite- or osumulite-like minerals based on the MinIdent program (D. Smith, pers. commun., 1990). Thus, alteration (i.e. hydration) of a primary phase such as cordierite or osumulite to a mixed assemblage of secondary clay-type minerals can account for the observed chemistry. In this regard it is interesting to note that Haslam (1983) reported an isotropic alteration product after cordierite with a composition not unlike that noted herein (see Figs. 10 and 11), albeit slightly Mg-deficient. Thus, we propose from this information that the ferromagnesian phase may represent altered cordierite. However, if one assumes that the variety of textural relationships all represent the same original phase rather than a variety of phases, then several generations of cordierite are required, some of which have not been observed in either igneous or metamorphic rocks based on our review of the literature. An alternative scenario, but one which we do not favour because of the added complexity, is that at least two different precursor mineral phases existed, one being cordierite and the second an unknown.

Discussion

The processes of magma mixing and commingling are generally well accepted in igneous petrology (e.g. Walker and Skelhorn, 1966; Anderson, 1976; Wiebe, 1973, 1992; Vernon, 1984, 1990) and they have been

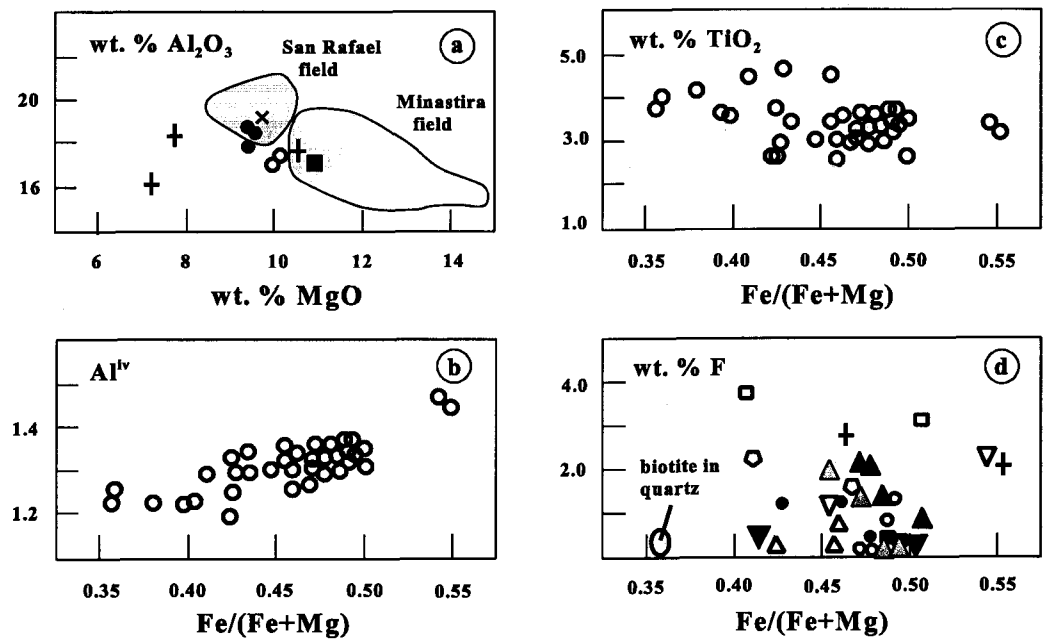

FIG. 9. Binary element diagrams summarizing the chemistry of biotite from the Minastira granite. (*a*) Al_2O_3 *vs.* MgO with bulk analyses for biotite separates for Miocene granites of SE Peru (Kontak, 1985) compared to the field for the Minastira granite. Also shown is the field of biotite composition for the San Rafael granite as determined from EMPA (unpubl. data of Kontak). (*b*) ^{iv}Al *vs.* Fe/(Fe+Mg); note that sample with extreme Fe-enrichment is in part chloritized and thus the Fe-enrichment may reflect secondary processes. (*c*) TiO_2 *vs.* Fe/(Fe+Mg). (*d*) F *vs.* Fe/Fe+Mg) for biotite grains with the analyses grouped according to individual grains (i.e. same symbol). Note the larger intra-grain variation with respect to both variables plotted.

documented in widely divergent settings (e.g. Castro *et al.* 1990; Feeley and Grunder, 1991; Seaman and Ramsey, 1992; Blake *et al.*, 1992; Stimac and Pearce, 1992). In fact, Castro *et al.* (1991), in recognizing the widespread occurrence of mixing and hybridiization within mafic–felsic systems, proposed a classifica-

TABLE 6. Representative analyses of apatite, Minastira granite, SE Peru

Point	3-35	3-36	3-53	3-54	3-55	3-73	3-74
SiO_2	0.25	0.22	ND	ND	ND	ND	ND
FeO	1.56	1.53	0.57	0.8	0.51	0.58	0.97
MnO	0.42	0.35	0.18	0.24	0.2	0.3	0.35
MgO	0.32	0.35	0.29	0.28	0.19	0.18	0.15
CaO	52.62	52.67	53.93	53.33	53.52	53.58	53.85
Na_2O	ND	ND	0.14	0.25	0.18	0.15	0.09
P_2O_5	42.29	42.12	42.31	42.26	42.4	42.2	42.44
Cl	0.48	0.52	0.32	0.4	0.28	0.29	0.27
F	2.27	2.02	2.79	2.43	2.45	2.29	2.4
Total	100.21	99.78	100.53	99.99	99.73	99.57	100.52
F, Cl=O	1.06	0.97	1.25	1.11	1.09	1.03	1.07
Total	99.15	98.81	99.28	98.88	98.64	98.54	99.45

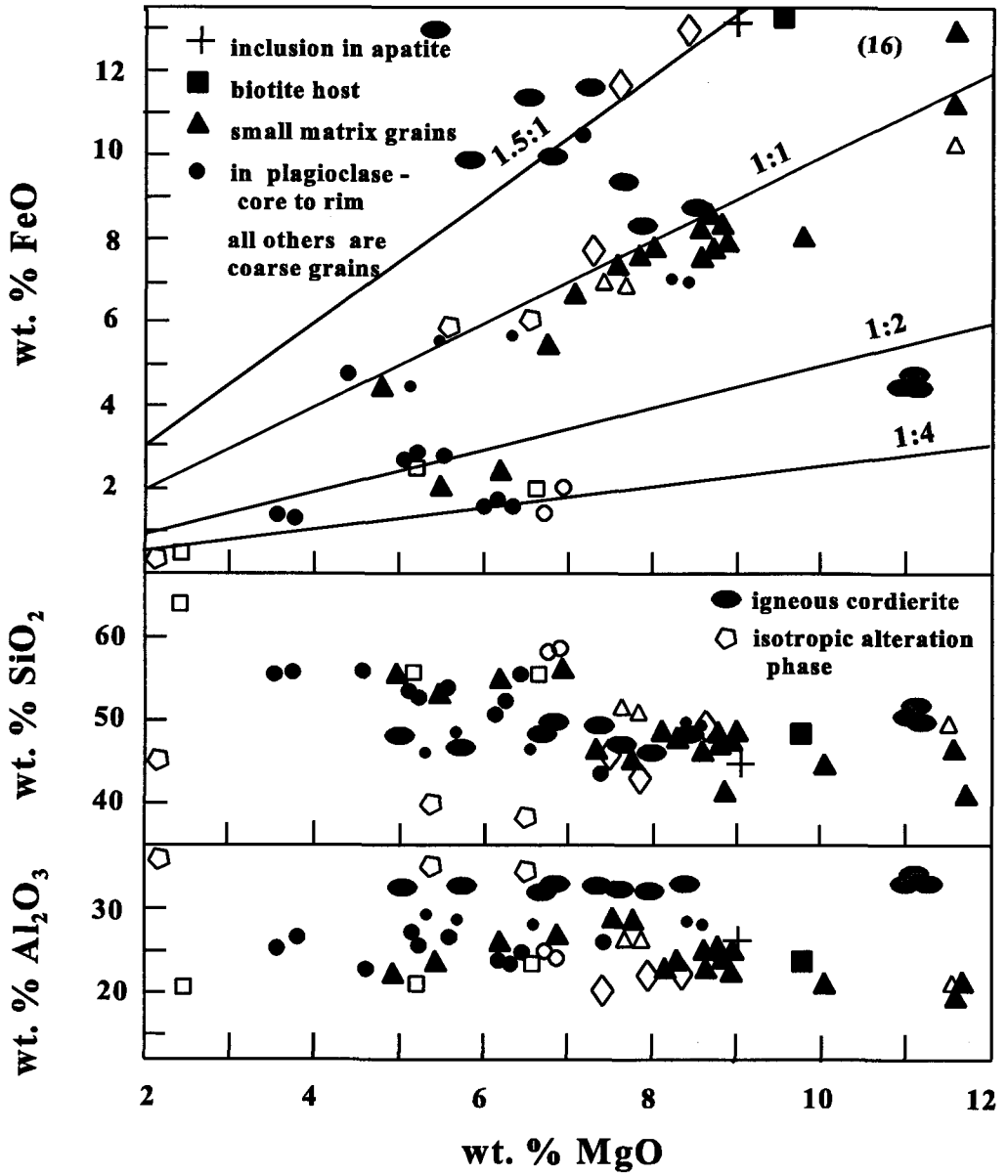

FIG. 10. Binary element diagrams for the brown and greenish-brown ferromagnesian phase in the Minastira granite with data also plotted for igneous cordierites from peraluminous intrusive and extrusive suites (Wyborn *et al.*, 1981; Allen and Barr, 1983; Maillet and Clarke, 1985; Maury *et al.*, 1985). The yellow isotropic phase, an alteration product after cordierite, is from Haslam (1983). Note that the most magnesian cordierites are from an andesite (Maury *et al.*, 1985) and thus reflect the magnesium-rich nature of the host.

tion scheme which takes into account the dominant process and end-member in such suites. In the following section we expand on some aspects of the petrology to develop a genetic model for the origin of the marked variability of textural and chemical features within these rocks.

TABLE 7. Representative analyses of unknown phase, Minastira granite, SE Peru

Point	1-45 light brown	1-47 dark brown	1-62 plag interior	2-33 plag interior	2-46 plag rim	4-11 apatite host
SiO_2	50.53	48.42	43.03	53.33	54.75	41.54
TiO_2	ND	ND	ND	ND	ND	ND
Al_2O_3	25.87	21.48	25.75	23.06	23.82	23.98
FeO	6.73	10.10	10.61	1.43	1.72	14.04
MgO	7.60	11.50	7.33	6.08	6.24	8.86
CaO	0.20	0.31	0.70	0.23	0.33	1.47
Na_2O	0.44	0.58	0.27	0.22	0.21	0.27
K_2O	0.33	0.32	0.30	0.28	0.29	0.16
MnO	ND	ND	ND	0.12	0.09	0.21
BaO	ND	ND	ND	0.16	ND	ND
Total	91.70	92.71	87.99	84.91	87.45	90.53

Point	3-26 plag rim	1-7 matrix grain	1-53 light brown	1-55 light brown	1-56 light brown	4-117 biotite host
SiO_2	43.22	40.89	49.23	47.58	45.95	43.93
TiO_2	0.18	ND	ND	ND	ND	ND
Al_2O_3	22.76	19.16	28.34	28.19	28.34	23.65
FeO	12.96	15.95	5.51	4.47	7.02	3.72
MgO	8.31	11.63	5.90	5.64	8.63	9.68
CaO	ND	ND	ND	ND	ND	ND
Na_2O	0.82	0.26	0.56	0.53	0.27	0.48
K_2O	0.22	0.25	0.50	0.29	0.35	1.09
MnO	0.26	0.24	0.38	0.29	0.11	0.18
BaO	0.09	0.26	ND	ND	0.10	ND
Total	88.82	88.64	90.42	86.99	90.77	82.73

Evidence for magma mixing. The occurrence of magma mixing at Minastira can be inferred from the mineralogy and whole-rock and mineral chemistry. Several textural features present in the Minastira rocks are frequently cited as being suggestive, if not diagnostic, of magma mixing, viz. sieved plagioclase (MacDonald and Katsura, 1965; Eichelberger, 1975, 1978; Kawamoto, 1992), resorption features such as embayed quartz (Smith and Carmichael, 1968; Sakuyama, 1978), internally fractured quartz (Kontak *et al.*, 1986), pyroxene coronas mantling quartz (Eichelberger, 1978; Stimac and Pearce, 1992), melt inclusions of mixed chemistry (Anderson, 1976) and disequilibrium or mixed mineral associations (Eichelberger, 1975; Sakuyama, 1978; Gerlach and Groves, 1982; Gourgraud *et al.*, 1989; O'Brien *et al.*, 1988). We also infer that the internal features of the biotite suggest incipient melting by analogy with other magmatic suites (e.g. Nixon, 1988; Stimac and Pearce, 1992) and direct comparison with experimental work of biotite stability in felsic systems (e.g., Clemens and Wall, 1981); therefore, biotite textures also support magma mixing and commingling. Chemical features of plagioclase that indicate mixing are compositional reversals, polymodal compositions and spikes in the zoning profiles (cf. Gourgaud and Villemant, 1992; Gourgaud *et al.*, 1989; Vogel *et al.*, 1987; Castro *et al.*, 1990).

The bulk chemistry of the samples examined, in particular the A/CNK values and the chondritic *REE* pattern, contrast with values and patterns typical of similar age granitic rocks in the area (e.g. San Rafael granite; Kontak and Clark, 1988). The highly peraluminous nature of the samples is anomalous and presumably reflects the abundance of the brown ferromagnesian phase (cordierite ?), whereas ΣREE is notably depressed compared to rocks of similar SiO_2 content in the area (Fig. 7) and is similar to that typical of intermediate volcanic rocks such as those of the Central Andes (e.g. Dostal *et al.*, 1977). The biotite chemistry is also unusual, the elevated MgO contents suggest equilibration with a relatively mafic melt. Nonetheless, the elevated F content of the biotite (to *c.* 4 wt.%) is more typical of highly evolved and volatile-rich felsic suites (Bailey, 1984). The heterogeneous distribution of F in biotite, which

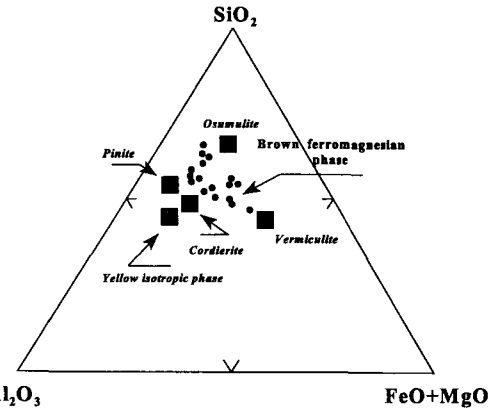

FIG. 11. Ternary plot (wt.%) for SiO_2–Al_2O_3–(FeO + MgO) showing the compositional range of the brown to greenish-brown alteration phase in relation to compositions of cordierite (as in Fig. 10), a yellow isotropic phase after cordierite (see text; Haslam, 1983), osumulite (Pichavant *et al.*, 1988*a*) and vermiculite and pinnite (from Deer *et al.*, 1966). Note that analyses of the brown ferromagnesian phase observed in the Minastira granite plot in a field defined by the phases mentioned.

is not unlike that noted by Pichavant *et al.* (1988*a*) for biotites in the Macusani volcanics, is matched by the wide range of plagioclase compositions and textures and the local enrichment of this mineral in BaO (to 1.3 wt.%).

Despite the non-exposure of cuspate interfaces between relatively mafic and felsic end members (see discussion below) that is common in the subvolcanic environment where magma commingling occurs (e.g. Castro *et al.*, 1990; De'Lemos, 1992; Wiebe, 1973, 1979, 1992; Vernon, 1983), the aforementioned features are clearly sufficient to indicate the occurrence of magma mixing at Minastira. The nature and origin of the end member components remains problematic, however.

Model for genesis of the subvolcanic Minastira granite. Several features that are of particular importance in terms of understanding the origin of the Minastira granite include: (1) fracturing or breakage of minerals, plausibly due to rupturing of melt inclusions during decompression of the magma; (2) internal fracturing of quartz that suggests thermal shock; (3) internal melting of biotite (e.g. Stimac and Pearce, 1992; Nixon, 1988); (4) internal melting of both alkali and plagioclase feldspar; (5) heterogeneous mineral chemistry as noted, for example, in biotite; (6) the abundance of a ferrromagnesian phase that may represent precursor cordierite; (7) a quenched matrix ranging in composition from *c.* 66 wt.% SiO_2 to nearly pure SiO_2, with the siliceous end member containing significant amounts of alkalis and Al_2O_3; and (8) minor amounts of plagioclase with concentrically-arranged inclusions of sillimanite and biotite and micro-inclusion rich apatite. On the basis of the aforementioned features the following petrological model is proposed.

Generation of at least two diverse melts occurred at depth with subsequent mixing of the two as a result of favourable melt densities and temperature (e.g. Sparks and Marshall, 1986). From the nature of the crystal assemblage and the matrix we can identify one end member as being felsic, probably rhyolitic in nature. The presence of concentrically-arranged sillimanite needles and rare biotite within plagioclase cores, rare sillimanite as constituents of plagioclase fragments, and coarse micro-inclusion-rich apatite suggest that such felsic melts may have originated from crustal fusion, perhaps similar to the slightly younger Miocene-age, peraluminous Macusani volcanics just to the north where similar textures are observed (Pichavant *et al.*, 1988*a,b*). Assuming that cordierite was indeed present in the melt, then this phase is inferred to be early magmatic based on the frequent euhedral shapes and occurrence as inclusions in quartz and feldspars. In this regard the cordierite conforms to Clarke's (1995) Type 2(c) cotectic cordierite. Hercinitic spinel is also interpreted as an early phase based on its occurrence, i.e. a loose spatial relationship to the cordierite phase and as inclusions within plagioclase. Thus, generation of the felsic melt is restricted to upper crustal levels (i.e., $\leqslant$4–5 kbar) and maximum temperatures of *c.* 800–900°C based on the presence of the cordierite phase, hercinitic spinel and F-rich nature of some of the biotite (Clemens and Wall, 1981; Pichavant *et al.*, 1988*a* and references therein). The compositions of inclusion free, euhedral to subhedral plagioclase of clear magmatic origin is consistent with a basaltic andesitic composition for the mafic melt. The absence of ubiquitous pyroxene coronas mantling quartz, as seen in the shoshonites at nearby Moromoroni (Kontak *et al.*, 1986), implies that the mafic component was subordinate to the felsic melt. The textures within biotite that suggest incipient breakdown would be consistent with superheating of the felsic melt and its phenocrystic assemblage due to mixing with resultant magma temperatures close to or exceeding that required for biotite breakdown (i.e. 900° to 950°C; Clemens and Wall, 1981).

Mixing of the two melts must have occurred prior to emplacement at the present level for the following reasons: (1) rapid crystallization is implied based on the grain size and textures within the matrix (Fig. 3); (2) the absence of enclaves or globules of mafic composition; (3) inclusions of glomeroclasts containing intergrown sieve-textured plagioclase; (4) complex textural relationship between plagioclase

and the brown ferromagnesian phase with both phases mantling each other. Although not indicative of relative timing or location of mixing, the abundance of internal fractures within quartz may be a result of thermal shock. The generally fractured and broken nature of crystals may have originated during convection (i.e. turbulent) within a magma chamber or during passage through a conduit, the latter fitting in with the mechanism suggested by Blake and Campbell (1986) for magma mixing. However, an alterative mechanism for fracturing of phenocrysts recently discussed by Best and Christiansen (1997) relates rupturing of crystals to vesiculation of melt that was trapped at higher pressures as inclusions within phenocrysts. Thus, crystallization of some of the phenocrystic component at a different level is suggested and residence within the area of mixing, most probably within the upper crust, must have occurred. The extent of residence time has been estimated by various workers based on diffusivities in Fe–Mg minerals (e.g. Gerlach and Groves, 1982) or dissolution rates in development of sieve-textured plagioclase based on experimental (Lofgren and Norris, 1981) and theoretical (Andersson and Eklund, 1994) work. Intervals calculated are of the order of a few hours to hundreds of hours and suggest relatively rapid post-mixing eruption where volcanic rocks have been the focus of study. The general absence of sodic-rich mantles on plagioclase despite the occurrence of such compositions in the matrix are taken to indicate that quenching occurred before reaction between crystals and melt could take place. Final emplacement of the mixed melt, within a narrow conduit at shallow levels, resulted in quenching of the magma and preservation of the disequilibrium assemblage.

Implications for genesis of granites of the Inner Arc region of SE Peru. As discussed elsewhere (Kontak *et al.*, 1984, 1986; Kontak and Clark, 1988), the close spatial and temporal association of shoshonitic magmatism and peraluminous granites of latest Oligocene age in the Cordillera Oriental region of SE Peru suggests a cause and effect relationship. Although the mafic component of the Minastira system cannot be identified unambiguously, the nearby *c.* 25 Ma Moromoroni shoshonites are of appropriate age, as are other centres of mafic magmatism in this part of the Cordillera Oriental (Sandeman, 1995; Sandeman *et al.*, 1995), and indicate that at this time mantle-derived magmas ascended to shallow crustal levels and prompted the advection of heat and volatiles into upper crustal levels. The latter phenomenon would have promoted the melting of parts of the thick metasedimentary sequence that characterizes the Inner Arc region of the Central Andes, which is dominated by pelitic sequences (Laubacher, 1978), and thus given rise to the strongly peraluminous cordierite ± sillimanite granites such as occur at nearby San Rafael. In this context, the intimate interplay of mafic–felsic magmatism documented here is similar to that documented throughout much of the geological record for both intrusive and extrusive igneous rocks (Anderson, 1976; Castro *et al.*, 1991).

Conclusions

The Minastira granite, a subvolcanic plug of fine-grained granitic rock, has preserved textures indicative of a history involving mixing of at least two magmas, a volumetrically dominant felsic component, which is in part restitic, and a less voluminous mafic one. The felsic melt is represented by variably fractured, altered and embayed crystals of quartz, feldspar and biotite, with minor coarse-grained and melt- and fluid-inclusion rich apatite, and possible cordierite, whereas the mafic melt is represented by calcic plagioclase and rare pyroxene mantles on quartz. The process of magma mixing is reflected in the ubiquitous presence of sieve-textured plagioclase with complex textural relationships. The absence of mafic enclaves indicates that physico-chemical conditions of the mixing were conducive to homogenization (i.e. chemical diffusion) and an apparently homogeneous rock is now observed. The combination of glomeroclasts of crystals that originated from both the mafic and felsic end members, and a quenched quartz-feldspar matrix indicate that the mixing occurred in an underlying magma chamber and that the Minastira granite may have been a conduit or plug.

Acknowledgements

This research was conducted while the senior author was a graduate student at Queen's University and involved in the Central Andean Metallogenetic Project (1979–1984). Field work in Peru and laboratory studies supported by the Natural Sciences and Engineering Research Council of Canada (grant to A.H. Clark). The field work was carried out with the logistical assistance of Minsur S.A., through the good offices of F. Zavaleta. Mr. B. McKay, Dalhousie University, is acknowledged for providing assistance with the electron microprobe work. The authors appreciate the comments of journal reviewers that resulted in clarification and improvement of the text.

References

Allen, P.L. and Barr, S.M. (1983) The Ellison Lake pluton: a cordierite-bearing monzogranitic intrusive body in southwestern Nova Scotia. *Canad. Mineral.*,

21, 583–90.

Anderson, A.T. (1976) Magma mixing: petrological process and volcanological tool. *J. Volcan. Geoth. Res.*, **1**, 3–33.

Andersson, U.B. and Eklund, O. (1994) Cellular plagioclase intergrowths as a result of crystal-magma mixing in the Proterozoic Åland rapakivi batholith, SW Finland. *Contrib. Mineral. Petrol.*, **117**, 124–36.

Bailey, S.W. (1984) Crystal chemistry of the true micas. In *Micas* (S.W. Bailey, ed.), *Amer. Mineral.*, **13**, 13–60.

Best, M.G. and Christiansen, E.H. (1997) Origin of broken phenocrysts in ash-flow tuffs. *Geol. Soc. Amer. Bull.*, **109**, 63–73.

Blake, S. and Campbell, I.H. (1986) The dynamics of magma-mixing during flow in volcanic conduits. *Contrib. Mineral. Petrol.*, **94**, 72–81.

Blake, S., Wilson, C.J.N., Smith, I.E.M. and Walker, G.P.L (1992) Petrology and dynamics of the Waimihia mixed magma eruption, Taupo Volcano, New Zealand. *J. Geol. Soc. Lon.*, **149**, 193–207.

Castro, A., Moreno-Ventas, I., and de la Rosa, J.D. (1991) H-type (hybrid) granitoids: a proposed revision of the granite-type classification and nomenclature. *Earth Sci. Rev.*, **31**, 237–53.

Castro, A., de la Rosa, J.D. and Stephens, W.E. (1990) Magma mixing in the subvolcanic environment: petrology of the Gerena interaction zone near Seville, Spain. *Contrib. Mineral. Petrol.*, **105**, 9–26.

Clark, A.H., Palma, V.V., Archibald, D.A., Farrar, E. Arenas, M.J. (1983) Occurrence and age of tin mineralization in the Cordillera Oriental, southern Peru. *Econ. Geol.*, **70**, 514–20.

Clark, A.H., Kontak, D.J. and Farrar, E. (1984) A comparative study of the metallogenetic and geochronological relationships in the northern part of the Central Andean tin belt, SE Peru and NW Bolivia. In *Proceedings Sixth Quadrennial I.A.G.O.D. Symposium*. E. Schweizerbart'sche Verlags, Stuttgart, Germany, 269–79.

Clark, A.H., Farrar, E., Kontak, D.J., Langridge, R.J., Arenas, M.J., France, L.J, McBride, S.L., Woodman, P.L., Wasteneys, H.A., Sandeman, H.A. and Archibald, D.A. (1990*a*): Geologic and geochronologic constraints on the metallogenic evolution of the Andes of southeastern Peru. *Econ. Geol.*, **85**, 1520–83.

Clark, A.H., Kontak, D.J. and Farrar, E. (1990*b*) The San Judas Tadeo W (-Mo-Au) deposit: Permian lithophile metal mineralization in southeastern Peru. *Econ. Geol.*, **85**, 1651–68.

Clarke, D.B. (1995) Cordierite in felsic igneous rocks: a synthesis. *Mineral. Mag.*, **59**, 311–25.

Clemens, J.D. and Wall, V.J. (1981) Origin and crystallization of some peraluminous (S-type) granitic magmas. *Canad. Mineral.*, **19**, 111–32.

De'Lemos, R.S. (1992) Magma-mingling and melt modification between granitic pipes and host diorite, Guernsey, Channel Islands. *J. Geol. Soc. Lon.*, **149**, 709–20.

Deer, W.A., Howie, R.A. and Zussman, J. (1966) *An Introduction to the Rock-forming Minerals*. Longman, London, 528 p.

Dostal, J., Zentilli, M., Caelles, J.C. and Clark, A.H. (1977) Geochemistry and origin of volcanic rocks of the Andes (26°–28° S). *Contrib. Mineral. Petrol.*, **63**, 267–76.

Eichelberger, J.C. (1975) Origin of andesite and dacite: evidence of mixing at Glass Mountain in California and at other circum-Pacific volcanoes. *Bull. Geol. Soc. Amer.*, **86**, 1381–91.

Eichelberger, J.C. (1978) Andesites in island arcs and continental margins: relationship to crustal evolution. *Bull. Volcan.*, **41**, 480–500.

Feeley, T.C. and Grunder, A.L. (1991) Mantle contribution to the evolution of Middle Tertiary silicic magmatism during early stages of extension: the Egan Range volcanic complex, east-central Nevada. *Contrib. Mineral. Petrol.*, **106**, 154–69.

Fryer, B.J. (1977) Rare-earth evidence in iron formation for changing Precambrian oxidation states. *Geochim. Cosmochim. Acta*, **41**, 361–7.

Gerlach, D.C. and Groves, T.L. (1982) Petrology of Medicine Lake Highland volcanics: Characterization of endmembers of magma mixing. *Contrib. Mineral. Petrol.*, **80**, 147–59.

Gourgaud, A., Fichaut, M. and Joron, J.L. (1989) Magmatology of Mt. Pelée (Martinique, F.W.I.). I: Magma mixing and triggering of the 1902 and 1929 Pelean nuées ardentes. *J. Volcan. Geoth. Res.*, **38**, 143–69.

Gourgaud, A. and Villemant, B. (1992) Evolution of magma mixing in an alkaline suite: the Grande Cascade sequence (Monts-Dore, French Massif Central). Geochemical modelling. *J. Volcan. Geoth. Res.*, **52**, 255–75.

Haslam, H.W. (1983) An isotropic alteration product of cordierite. *Mineral. Mag.*, **47**, 238–40.

Injoque, J., Miranda, C., Carlier, G., Sologuren, W. and Tijero, L. (1983) Evidencia de basamento Pre-Cambriano en la región Inchupalla - Puno. *Boletin de la Sociedad Geológica del Perú*, No. **70**, 25–8.

Ishihara, S. (1977) The magnetite-series and ilmenite-series granitic rocks. *Mining Geology*, **27**, 293–305.

Kawamoto, T. (1992) Dusty and honeycomb plagioclase: indicators of processes in the Uchino stratified magma chamber, Izu Peninsula, Japan. *J. Volcan. Geoth. Res.*, **49**, 191–208.

Kontak, D.J. (1985) *The magmatic and metallogenetic evolution of a craton-orogen interface: the Cordillera de Carabaya, Central Andes, S.E. Peru.* Unpubl. Ph.D. thesis, Queen's University, Kingston, Ontario, 714 p.

Kontak, D.J., Clark, A.H. (1988) Exploration criteria for

tin and tungsten mineralization in the Cordillera Oriental of southeastern Peru. In *Granite-Related Mineral Deposits* (R.P. Taylor and D.F. Strong, eds.), Canadian Institute of Mining and Metallurgy, Special Volume **39**, 157–69.

Kontak, D.J., Clark, A.H. and Farrar, E. (1984) The magmatic evolution of the Cordillera Oriental, southeastern Peru. In *Andean Magmatism: Chemical and Isotopic Constraints* (R.S. Harmon and B.A. Barreiro, eds.), Nantwich, Shiva Publishing Ltd., 203–19.

Kontak, D.J., Clark, A.H., Farrar, E. and Strong, D.F. (1985) The rift-associated Permo-Triassic magmatism of the Eastern Cordillera: A precursor to the Andean orogeny. In *Magmatism at a Plate Edge: The Peruvian Andes* (W.S. Pitcher, M.P. Atherton, E.J. Cobbing and R.D. Beckindale, eds.), Blackie & Sons, Glasgow, 36–44.

Kontak, D.J., Clark, A.H., Farrar, E., Pearce, T.H., Strong, D.F. and Baadsgaard, H. (1986) Petrogenesis of a Neogene shoshonite suite, Cerro Moromoroni, Puno, S.E. Peru. *Canad. Mineral.*, **24**, 117–35.

Kontak, D.J., Clark, A.H., Farrar, E., Archibald, D.A. and Baadsgaard, H. (1987) Geochronologic data for Tertiary granites of the southeast Peru segment of the central Andean tin belt. *Econ. Geol.*, **82**, 1611–8.

Kontak, D.J., Clark, A.H., Farrar, E., Archibald, D.A. and Baadsgaard, H. (1990) Late Paleozoic-Early Mesozoic magmatism in the Cordillera de Carabaya, Puno, southeastern Peru: Geochronology and petrochemistry. *J. South American Earth Sciences*, **3**, 213–30.

Laubacher, G. (1978) *Géologie de la Cordillère Orientale et l'Altiplano au nord et au nor-ouest du Lac Titicaca (Pérou)*. Unpubl. Ph.D. thesis, ORSTOM, Paris, 95, 217 p.

Lofgren, G. and Norris, P.N. (1981) Experimental duplication of plagioclase sieve and overgrowth textures. (Abstract) Geological Society America Abstracts with Program, 13, 498.

London, D. (1992) Phosphorous in S-type magmas: the P_2O_5 content of feldspars from peraluminous granites, pegmatites and rhyolites. *Amer. Mineral.*, **77**, 126–45.

London, D., Morgan, G.B. VI, Babb, H.A. and Loomis, J.L. (1993) Behaviour and effects of phosphorus in the system Na_2O-K_2O-Al_2O_3-SiO_2-P_2O_5-H_2O at 200 MPa (H_2O). *Contrib. Mineral. Petrol.*, **113**, 450–65.

MacDonald, G.A. and Katsura, T. (1965) Eruption of Lassen Peak, Cascade Range, California, in 1915: Example of mixed magmas. *Bull. Geol. Soc. Amer.*, **76**, 475–482.

Maillet, L.A. and Clarke, D.B. (1985) Cordierite in the peraluminous granites of the Meguma Zone, Nova Scotia, Canada. *Mineral. Mag.*, **49**, 695–702.

Maury, C., Clocchiatti, R., Coulon, C., D'Arco, P. and Westercamp, D. (1985) Signification du grenat et de la cordiérite dans les laves du Sud-Ouest martiniquais. *Bullétin de Minéralogie*, **108**, 63–79.

Muecke, G.K. and Clarke, D.B. (1981) Geochemical evolution of the South Mountain batholith, Nova Scotia: rare earth element evidence. *Canad. Mineral.*, **19**, 133–46.

Nixon, G. (1988) Petrology of the younger andesites and dacites of Iztaccihatl volcano, Mexico: II. Chemical stratigraphy, magma mixing and the composition of basaltic liquid influx. *J. Petrol.*, **29**, 265–303.

O'Brien, H.E., Irving, A.J. and McCallum I.S. (1988) Complex zoning and resorption of phenocrysts in mixed potassic mafic magmas of the Highwood Mountains, Montana. *Amer. Mineral.*, **73**, 1007–24.

Palma, V.V. (1981) *The San Rafael tin-copper deposit, SE Peru*. Unpublished M.Sc. thesis, Queen's University, Kingston, Ontario, 235 p.

Pichavant, M., Kontak, D.J., Valencia Herrera, J. and Clark, A.H. (1988*a*) The Miocene-Pliocene Macusani volcanics, SE Peru. I Mineralogy and magmatic evolution of a two-mica aluminosilicate-bearing ignimbrite suite. *Contrib. Mineral. Petrol.*, **100**, 300–24.

Pichavant, M., Kontak, D.J., Briqueu, L., Valencia Herrera, J. and Clark, A.H. (1988*b*) The Miocene-Pliocene Macusani volcanics, SE Peru. II Geochemistry and origin of a felsic peraluminous magma. *Contrib. Mineral. Petrol.*, **100**, 325–38.

Pichavant, M., Montel, J.M., and Richard, L.R. (1992) Apatite solubility in peraluminous liquids: experimental data and an extension of the Harrison-Watson model. *Geochim. Cosmochim. Acta*, **56**, 3855–61.

Pitcher, W.S., Atherton, M.P., Cobbing, E.J. and Beckinsale, R.D. (eds.) (1985): *Magmatism at a Plate Edge*. Blackie and Sons Ltd.

Sakuyama, M. (1978) Petrographic evidence of magma mixing in Shirouma-Oike Volcano, Japan. *Bull. Volcan.*, **41**, 501–12.

Sandeman, H.A. (1995) *Lithostratigraphy, petrology and geochronology of the Crucero Supergroup, Puno, SE Peru: implications for the Cenozoic geodynamic evolution of the southern Peruvian Andes*. Unpubl. PhD thesis, Queen's University, Kingston, Ontario, 382 pp.

Sandeman, H.A., Clark, A.H. and Farrar, E. (1995) An integrated tectono-magmatic model for the evolution of the southern Peruvian Andes (13–20°S) since 55 Ma. *International Geology Reviews*, **37**, 1039–73.

Sandeman, H.A., Clark, A.H., Farrar, E. and Arroyo, G. (1996*a*) The Crucero Supergroup, Puno Department, SE Peru: (i) lilthostratigraphy, petrology and $^{40}Ar/^{39}Ar$ geochronology of the Picotani Group. *J. South American Earth Sciences* (submitted).

Sandeman, H.A., Clark, A.H., Farrar, E. and Arroyo, G. (1996*b*) The Crucero Supergroup, Puno Department, SE Peru: (i) lilthostratigraphy, petrology and $^{40}Ar/^{39}Ar$ geochronology of the Quenamari Group.

J. South American Earth Sciences (submitted).

Sato, H. (1975) Diffusion coronas around quartz xenocrysts in andesites and basalts from Tertiary volcanic region in northeastern Shikoku, Japan. *Contrib. Mineral. Petrol.*, **50**, 40–64.

Seaman, S.J. and Ramsey, P.C. (1992) Effects of magma mingling in the granites of Mount Desert Island, Maine. *J. Geol.*, **100**, 395–409.

Smith, A.L. and Carmichael, I.S.E. (1968) Quaternary lavas from the southern Cascades, western U.S.A. *Contrib. Mineral. Petrol.*, **19**, 212–38.

Sparks, R.S.J. and Marshall, L.A. (1986) Thermal and mechanical constraints on mixing between mafic and silicic magmas. *J. Volcan. Geoth. Res.*, **29**, 99–124.

Stimac, J.A. and Pearce, T.H. (1992) Textural evidence of mafic-felsic magma interaction in dacitic lavas, Clear Lake, California. *Amer. Mineral.*, **77**, 795–809.

Vernon, R.H. (1983) Restite, xenoliths and microgranitoid enclaves in granites. *Journal Proceedings Royal Society of New South Wales*, **116**, 77–103.

Vernon, R.H. (1990) Crystallization and hybridism in microgranitoid enclaves: Microstructural evidence. *J. Geophys. Res.*, **95**, 17849–59.

Vogel, T.A., Ryerson, F.J., Noble, D.C. and Younker, L.W. (1987) Limits to magma mixing based on chemistry and mineralogy of pumice fragments erupted from a chemically zoned magma body. *J. Geol.*, **95**, 659–70.

Walker, G.P.L. and Skelhorn, R.R. (1966) Some associations of acid and basic igneous rocks. *Earth-Science Reviews*, **2**, 93–109.

White, A.J.R. and Chappell, B.W. (1983) Granitoid types and their distribution in the Lachlan Fold Belt, southeastern Australia. In *Circum-Pacific Granitoid Terranes* (J.A. Roddick, ed.), Geological Society of America Memoir **159**, 21–34.

Wiebe, R.A. (1973) Relations between coexisting basaltic and granitic magmas in a composite dike. *Amer. J. Sci.*, **273**, 130–51.

Wiebe, R.A. (1979) Commingling of contrasted magmas in the plutonic environment: examples from the Nain Anorthositic Complex. *J. Geol.*, **88**, 197–209.

Wiebe, R.A. (1992) Basaltic injections into floored silicic magma chambers. *Trans. Amer. Geophys. Union*, **74**, No. 1, 1–3.

Yamamura, B. (1991) *The Palca 11 tungsten deposit and associated granitoid rocks, Choquene district, Puno, southeastern Peru.* Unpublished M.Sc. thesis, Queen's University, Kingston, Ontario, Canada, 255 p.

Wyborn, D., Chappell, B.W. and Johnson, R.M. (1981) Three S-type volcanic suites from the Lachlan Fold Belt, Southeast Australia. *J. Geophys. Res.*, **86**, 10335–48.

[*Manuscript received 10 November 1996: revised 16 April 1997*]